Localization of Hydrons in Hydrogen Bonds Using Dipolar Solid State NMR Spectroscopy

Christof-G. Hoelger and Hans-Heinrich Limbach*

Institut für Organische Chemie, Takustrasse 3, Freie Universität Berlin, D-14195 Berlin, FRG

Received: July 27, 1994[⊗]

In this paper, the possibility of obtaining information on the structure and dynamics of hydrogen bonds by studying heteronuclear dipolar interactions with mobile hydrons, i.e. protons and especially deuterons, is explored. The study of dipolar interactions with deuterons has several advantages. Firstly, high resolution is easily achieved because broad-band ^1H decoupling can be applied without removing the dipolar interaction to the deuterated site of interest. Secondly, deuteration of mobile proton sites can easily be achieved; the selectivity is enhanced by additional ^{13}C or ^{15}N labeling. Thirdly, it becomes possible to measure hydrogen deuterium isotope effects on hydrogen bond distances if the corresponding dipolar coupling to ^1H can also be determined. In this paper, the $^{15}N-^2H$ (≡ND) interaction in static samples of ^{15}N-enriched organic polycrystalline powders is studied by ^{15}N CP NMR line-shape analysis (CP: cross polarization) after establishing the parameters of the chemical shift anisotropy from experiments performed on the protonated species. This method is particularly suitable for variable temperature studies as required in the case of hydrogen-bonded systems with mobile deuterons. As examples, three compounds typical for various situations were studied: The trimethylammonium chloride $(CD_3)_3{}^{15}N-H\cdots Cl$ (**1a**) and $(CH_3)_3{}^{15}N-D\cdots Cl$ (**1b**) were chosen as examples of N—L···X hydrogen-bonded systems (L = H, D), exhibiting an H/D isotope effect on the NL distance. Dimethyldibenzotetraaza[14]annulene-$^{15}N_4$ (**2**) represents the case of N—L···N hydrogen bonds with mobile deuterons. Finally, α-glycine, $^-OOCCH_2{}^{15}NL_3{}^+$ (**3**) was studied as an example where more than one hydrogen isotope is bound to ^{15}N and where rotational jumps occur around the $C-{}^{15}N$ axis. Depending on the number of deuterons, multiplets of differing orders could be observed in the ^{15}N CP NMR spectra. These multiplets contain information concerning the localization and the mobility of the ammonium deuterons. The results obtained agree well with those obtained by other methods.

Introduction

A major problem in hydrogen bond research is the localization of the hydrogen bond proton.[1] This is due to the high proton mobility and because of experimental difficulties in the determination of bond lengths involving hydrogen by X-ray diffraction.[2] Precise hydrogen bond geometries can be obtained by neutron diffraction, but this technique generally requires relatively large single crystals.[2] Interesting information on the vibrational states of protons in hydrogen bonds is also obtained by IR and Raman spectroscopy[1] and by inelastic neutron scattering.[3] Potentially, replacement of protons by deuterons can lead to interesting effects on heavy atoms hydrogen bond distances[4] and vibrational frequencies[5] from which information about the potential of the hydrogen motion can be obtained.

From a theoretical standpoint, all methods which provide information on the localization and transfer of protons and deuterons in hydrogen bonds are of great interest. In the case of weak hydrogen bonds, where the protons move in double wells, variable temperature high-resolution solid state NMR under the conditions of cross polarization (CP) and magic angle spinning (MAS) has proven to be useful for the study of rate constants of proton and deuteron transfer. This method relies on modulations of the isotropic nuclear chemical shifts of spin 1/2 nuclei such as ^{13}C or ^{15}N, etc., during the transfer processes studied. Rate constants in the second time scale are obtained by magnetization transfer,[10a] in the millisecond time scale by line-shape analysis,[6-9] and in the micro- to nanosecond time scale by analysis of longitudinal relaxation times.[10b]

However, NMR offers additional possibilities which may be potentially useful in the study of hydrogen-bonded systems even in cases where the barrier of proton transfer is small or absent. We refer here to techniques of obtaining heteronuclear distances in organic compounds by studying specific nuclear dipolar interactions D_{SI} between the spins S and I in the solid state.[11-14] It is well-known that D_{SI} is proportional to $r_{SI}{}^{-3}$, where r_{SI} represents the distance between the two spins. The problem of dipolar NMR is (i) the resolution of dipolar interactions in different atomic sites of the sample, a problem especially in natural abundance ^{13}C NMR, (ii) the interference with the chemical shift anisotropy, (iii) the removal of undesired dipolar interactions, especially to protons, and (iv) nuclear and molecular motions which modulate the dipolar interactions. In the case of compounds whose NMR spectra are characterized only by one or two isotropic chemical shifts and where the dipolar interactions are large the latter can be elucidated by line-shape analysis of the spectra of static powders at variable temperatures or of slow spinning samples, taking into account the anisotropy of the chemical shifts. Thus, various heavy atom distances between ^{13}C, ^{15}N, and ^{31}P atoms have been obtained,[11a-d] as well as one distance between ^{15}N and a deuteron.[11e] In the case of dipolar couplings to protons a complication arises. The homonuclear dipolar coupling among the latter must be removed in order to obtain heteronuclear distances to specific proton sites. This can be done by applying multipulse techniques[12] which can be combined with slow MAS in order to obtain a chemical shift resolution. Griffin et al.[13] were able to determine $^{15}N-{}^1H$ distances in several organic polycrystalline solids. In recent years, further double and triple resonance multipulse NMR experiments with and without MAS were devised by Schaefer et al.[14] for the determination of heteronuclear dipolar couplings between spin 1/2 nuclei[14a-d] and between a spin 1/2 and a spin 1 nucleus.[14e] Thus, $^{13}C-{}^{15}N$ and $^{13}C-{}^2H$ distances as well

[⊗] Abstract published in *Advance ACS Abstracts,* October 1, 1994.

0022-3654/94/2098-11803$04.50/0

as $^{15}N-^{31}P$ distances[15] in organic and biochemical solids have been derived. Previous experiments concentrated on room temperature experiments on systems with restricted molecular, i.e. nuclear, mobilities. We are aware only of one exception, a combined multipulse/MAS study of an enzyme[15] at temperatures between −45 and −90 °C. Lower temperatures are very difficult to achieve by multipulse/MAS NMR. The problem is not low-temperature MAS itself—which also has been frequently applied in our laboratory[7−10]—but the need for very stable spinning speeds and an accurate multipulse tuning and calibration, which, from our own experience, is very difficult to achieve at low temperatures. For comparison with neutron inelastic scattering[3] even cryogenic sample temperatures are required.

The purpose of this paper is, therefore, to explore the problems of measuring dipolar interactions with mobile hydrogen isotopes in hydrogen bonds, with particular emphasis on the possibility of performing facile low-temperature experiments and the study of H/D isotope effects on the hydrogen bond geometries. In order to achieve these goals variable temperature ^{15}N CP NMR of ^{15}N- and ^{2}H-enriched static powders, where ^{15}N is directly involved in hydrogen bonding and where the chemical site resolution does not constitute a problem, was chosen.

The paper is organized as follows: After short theoretical and experimental sections we report on solid state ^{15}N NMR line-shape spectra and their analysis of several specifically ^{15}N and ^{2}H labeled model compounds. The first example is trimethylammonium hydrochloride (**1**), labeled with ^{15}N and with deuterium. More precisely, the compounds $(CD_3)_3{}^{15}NH^+Cl^-$ (**1a**) and $(CH_3)_3{}^{15}ND^+Cl^-$ (**1b**) were prepared and studied. The results are compared to those obtained by Griffin et al. for $(CH_3)_3{}^{15}NH^+Cl^-$. Next, the organic dye dimethyldibenzotetraaza[14]annulene was chosen as an example of a NH···N hydrogen-bonded system affected by proton tautomerism.[9a,10b] In this case, the experiments had to be performed at low temperatures, where the protons are localized. It is shown that not only the short distance but also the long nitrogen−hydrogen distance can be obtained. Finally, α-glycine ^{15}N-enriched in the ammonium position provided another example where variable temperature experiments are important. This compound was chosen because of (i) its model character for ammonium groups in side chains of proteins, (ii) the heteronuclear dipolar coupling of the ^{15}N nucleus with three hydrogen isotopes, and (iii) the modulation of the dipolar $^{15}N-^{2}H$ interaction by the ammonium group rotation. The rotation has been previously studied by neutron diffraction[16] and ^{2}H NMR techniques.[17]

Theoretical Section

The NMR theory of dipolar heteronuclear coupling has been described previously.[18] Therefore, its main results will be repeated here only very briefly, mainly in order to define the quantities obtained experimentally. Our interest is focused particularly on the calculation of the NMR line shapes of ^{15}N nuclei dipolar coupled to hydrogen isotopes which are embedded in multicrystalline powders. Both static powders and powders which slowly rotate at the magic angle are considered. The possibility of either slow or fast exchange between various molecular states is taken into account. In the following, the light hydrogen isotopes are abbreviated by the symbols L = H or ^{1}H, D or ^{2}H, and the ^{15}N nuclei as S = A, X, where A−L···X is the hydrogen bond studied.

As illustrated in Figure 1a, in a molecular frame of reference with the coordinates X, Y, and Z the orientation of the magnetic field vector B_0 is related to this frame by the angles θ and ϕ.

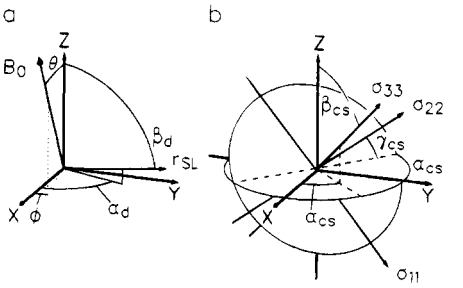

Figure 1. Explanation of angles used in eqs 3−8.

The orientation of the distance vector r_{SL} between S and L is given by the angles α_d and β_d. The principle components of the chemical shift tensor are labeled σ_{11}, σ_{22}, and σ_{33} (Figure 1b). Its orientation is given by the Euler angles α_{cs}, β_{cs} and γ_{cs}. If all angles are zero, $\sigma_{11} \parallel X$, $\sigma_{22} \parallel Y$, and $\sigma_{33} \parallel Z$. Any arbitrary orientation is then obtained as usual by three consecutive positive rotations, i.e. α_{cs} about σ_{11}, β_{cs} about σ_{22}, and γ_{cs} about σ_{11}.

The absorption frequency ν^S of the nucleus S in the state j embedded in a given crystallite then only depends on the angles θ and ϕ and the spin states of the dipolar-coupled hydrogen isotopes L, characterized by the magnetic quantum numbers m_L:

$$\nu^S(j,\theta,\phi) = \nu^S_{zee} + \nu^S_{cs}(j) + \sum_L m_L \nu^{SL}_d(j) \quad (1)$$

Here, $\nu_{zee} = \gamma_S B_0/2\pi$ represents the Zeeman frequency of S, ν^S_{cs} the contribution arising from the chemical shift anisotropy, m_L the magnetic quantum numbers of isotope L, and $\nu^{SL}_d(j)$ the contribution arising from dipolar coupling of S with spin L in the state j. In eq 1, heteronuclear scalar coupling and second-order dipolar coupling caused by the quadrupole moment of ^{2}H are neglected.[19,20] The contribution arising from the chemical shift anisotropy is given in the usual secular approximation by

$$\nu^S_{cs}(j) = (\gamma_S B_0/2\pi)\,(\sigma^S_{11}(j)\cos^2\theta^S_{11}(j) + \sigma^S_{22}(j)\cos^2\theta^S_{22}(j) + \sigma^S_{33}(j)\cos^2\theta^S_{33}(j)) \quad (2)$$

where $\theta^S_{ii}(j)$ is the angle between B_0 and $\sigma^S_{ii}(j)$. On inspection of Figure 1, it follows that

$$\cos\theta^S_{11}(j) = \cos\gamma^S_{cs}(j)\cos\beta^S_{cs}(j)\sin\theta\cos(\phi-\alpha^S_{cs}(j)) + \sin\gamma^S_{cs}(j)\sin\theta\sin(\phi-\alpha^S_{cs}(j)) - \cos\gamma^S_{cs}(j)\sin\beta^S_{cs}(j)\cos\theta \quad (3)$$

$$\cos\theta^S_{22}(j) = -\sin\gamma^S_{cs}(j)\cos\beta^S_{cs}(j)\sin\theta\cos(\phi-\alpha^S_{cs}(j)) + \cos\gamma^S_{cs}(j)\sin\theta\sin(\phi-\alpha^S_{cs}(j)) + \sin\gamma^S_{cs}(j)\sin\beta^S_{cs}(j)\cos\theta \quad (4)$$

$$\cos\theta^S_{33}(j) = \sin\beta^S_{cs}(j)\sin\theta\cos(\phi-\alpha^S_{cs}(j)) + \cos\beta^S_{cs}(j)\cos\theta \quad (5)$$

In the same frame of reference the contributions of the dipolar S−L coupling in eq 1 are given by

$$\nu^{SL}_d(j) = D_{SL}(j)\{1 - 3\cos^2\theta^{SL}_d(j)\} \quad (6)$$

$$D_{SL}(j) = (\gamma_S\gamma_L h\mu_0/16\pi^3)/r_{SL}{}^3(j) \quad (7)$$

$D_{SL}(j)$ is the dipolar coupling constant, $\theta^{SL}_d(j)$ is the angle between the SL vector and the magnetic field, γ_S and γ_L are the gyromagnetic ratios, μ_0 is the permeability, and h is Planck's

constant. From Figure 1 it follows that $\cos\theta_d^{SL}(j)$ is given by

$$\cos\theta_d^{SL}(j) = \sin\beta_d^{SL}(j)\sin\theta\cos(\phi - \alpha_d^{SL}(j)) + \cos\beta_d^{SL}(j)\cos\theta \quad (8)$$

In the presence of a fast dynamic exchange between different states the resulting frequency is simply obtained by

$$\nu^S(\theta,\phi) = \sum_j x(j)\,\nu^S(j,\theta,\phi) \quad (9)$$

where $x(j)$ is the mole fraction of state j. The powder spectrum of S is obtained from eqs 1−9 by calculating $\nu^S(\theta,\phi)$ for all orientations of the magnetic field, taken in increments of 1−2° for θ and ϕ. The corresponding signal intensities are given by the value of $\sin\theta$.

The solid state MAS NMR spectra of nuclei S, dipolar coupled to an isolated nucleus L under the conditions of slow sample rotation, can easily be calculated according to the method of Grant et al.[21] by defining a combined CSA/dipolar coupling tensor which has to be diagonalized numerically. With these effective diagonal tensor elements, the sideband intensities for each spin state m_L can then be calculated as usual by the method of Herzfeld and Berger.[22] Finally, the total spectrum is given by the sum of the subspectra arising from the different states m_L.

For the determination of S−L bond lengths, firstly the elements of the CSA tensor are conveniently obtained by simulation of the solid state NMR spectra of S of the protonated systems, i.e. L = H under ^{1}H decoupling. The remaining unknown parameters, i.e. the polar angles α_d^{SD} and β_d^{SD}, and the dipolar coupling constant D_{SD} are then determined by line-shape simulation of the spectra obtained without ^{1}H decoupling in the case of overall deuterated samples except in the hydrogen bond of interest or of the deuterated systems with L = D. It must be noted that the effective dipolar coupling represents an average over $1/(r_{SL})^3$ and $\cos^2\theta_d^{SL}$ within the NMR time scale. As a consequence, the distances derived from the dipolar coupling constants are found to be approximately 3% longer in comparison to data obtained by neutron diffraction techniques.[11g,13a,23]

Experimental Section

Isotopically labeled trimethylammonium chloride was synthesized from labeled precursors using literature procedures.[24] ^{15}N-labeled α-glycine was purchased from Chemotrade, Leipzig. The synthesis of isotopically labeled dimethyldibenzotetraaza-[14]annulene-$^{15}N_4$ has been reported elsewhere.[25] Deuteration in the mobile proton sites was achieved by dissolving the compounds in mixed organic liquids containing CH_3OD and evaporation of the solvent. Trimethylammonium chloride was dried by heating the sample in vacuum. To prevent reprotonation, the rotors were loaded under nitrogen and sealed.

The ^{15}N CP NMR measurements were performed at 9.12 MHz (2.1 T cryomagnet) and 30.41 MHz using the Bruker CXP 100 and MSL 300 NMR spectrometers. For the 30.41 MHz measurements a 5 mm DOTY high-speed CPMAS probe head was used and for the 9.12 MHz measurements a standard 7 mm Doty CPMAS probe. All spectra were referenced to external solid $^{15}NH_4Cl$ (95%). Spectral artifacts were minimized using a T_1 pulse sequence with 5 ms as waiting time.[26]

Results and Discussion

NH···X Hydrogen Bonds. Example: Trimethylammonium Chloride. In order to show that comparative ^{15}N−H distances and ^{15}N−D distances can be obtained by solid state ^{15}N NMR, we firstly report the results of a study on the dipolar ^{15}N−H and ^{15}N−D interaction in the trimethylammonium hydrochlorides $(CD_3)_3\,^{15}N{-}H{\cdots}Cl$ (**1a**) and $(CH_3)_3{}^{15}N{-}D{\cdots}Cl$ (**1b**). This system was chosen for several reasons: (i) the preparation of the labeled compounds is straightforward, (ii) the ^{15}N nucleus in these compounds exhibits only a very small chemical shift anisotropy, (iii) the compound exhibits a good sensitivity in the ^{15}N NMR experiment, and (iv) ^{15}N NMR experiments have been performed by Griffin et al.[13a] on $(CH_3)_3{}^{15}NH{\cdots}Cl$.

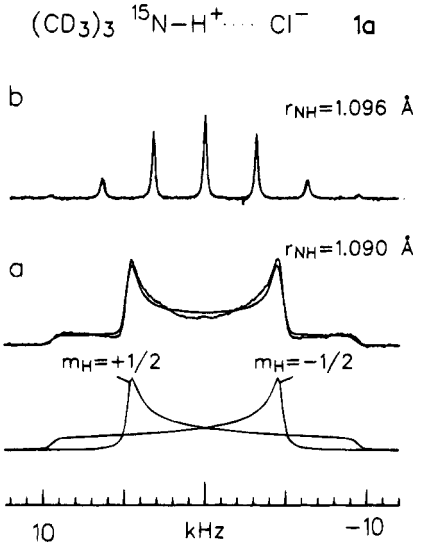

Figure 2. Superposed experimental and calculated 9.12 MHz ^{15}N CP NMR spectra of solid trimethylammonium chloride, $(CD_3)_3NH{\cdots}Cl$ (**1a**), obtained without ^{1}H decoupling of a static sample (a) and of a sample rotating slowly at the magic angle (b). The spectra were calculated as described in the text using the parameters $\sigma_{11} = \sigma_{22} = \sigma_{33} = -4$ ppm, $\sigma_{iso} = 4.2$ ppm, $\alpha_d = \beta_d = 0°$, and the distances indicated.

In Figure 2 are shown the superposed experimental and calculated room temperature ^{15}N CP NMR spectra of **1a**, obtained for the static powder (Figure 2a) and for slow MAS (Figure 2b) in the absence of ^{1}H decoupling. Since the ^{15}N chemical shift anisotropy is almost zero and homonuclear couplings among protons are small due to the deuteration of the methyl groups, the dipolar interaction between the ^{15}N nucleus and the attached proton in **1a** is the dominant contribution to the spectra of **1a**. This leads to a typical Pake doublet in the spectrum of the static powder and to a typical rotational sideband spectrum when the sample is spun slowly at the magic angle, as reported by Griffin et al.[13a] The Pake doublet consists of two subspectra arising from the different spin states $m_H = \pm 1/2$ of the hydrogen-bonded proton. The maxima stem from the molecules with the NH axis perpendicular to B_0, the shoulders from those with the NH axes parallel to B_0. For $(CH_3)_3{}^{15}NH^+{\cdots}Cl^-$, a similar sideband spectrum (Figure 2b) can be obtained under slow magic angle spinning conditions when homonuclear ^{1}H interactions are suppressed by ^{1}H multipulse decoupling.[13a] The latter, however, scales the width of the spectrum; the scaling fractor is determined in a separate experiment.

The ^{1}H-decoupled ^{15}N CP NMR spectrum of the static powder of **1b** is shown in Figure 3a. The spectrum consists of a superposition of three subspectra arising from the three spin states of the attached deuteron, as indicated. The state with $m_D = 0$ gives rise to the sharp center line which is not affected by dipolar coupling to the deuteron. This line is only affected by the almost imperceptible ^{15}N chemical shift anisotropy. The remaining two deuteron spin states with $m_D = \pm 1$ lead to a Pake subdoublet similar to the case of **1a**. We therefore call

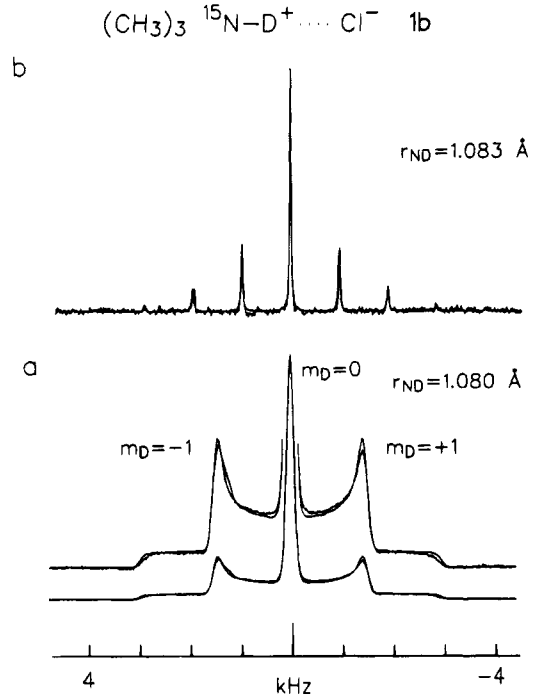

Figure 3. Superposed experimental and calculated 9.12 MHz ^{15}N CP NMR spectra of solid trimethylammonium chloride, $(CH_3)_3ND{\cdots}Cl$ (**1b**), obtained with ^1H decoupling of a static sample (a) and of a sample rotating slowly at the magic angle (b). The spectra were calculated as described in the text using the parameters $\sigma_{11} = \sigma_{22} = \sigma_{33} = -4$ pm, $\sigma_{iso} = 4.2$ ppm, $\alpha_d = \beta_d = 0°$, and the distances indicated.

the line shape of Figure 3a a "Pake triplet". In comparison to the maxima of the Pake doublet in Figure 2a, the frequency difference between the two outer maxima in Figure 3a is approximately reduced by a factor of $I_{2H}\gamma_{2H}/I_{1H}\gamma_{1H} = 0.307$, where I_L represents the spin quantum number of L. This circumstance, however, does not decrease the precision of the value r_{ND} because the residual line width in Figure 3a is smaller than in the case of Figure 2a. The reason for this finding is that couplings with the methyl deuterons are absent in **1b** and that dipolar $^{15}N-H$ couplings vanish because of ^1H decoupling. As can be inferred from Figures 2 and 3, the agreement between the experimental and the calculated spectra is absolutely satisfactory. The simulations of the spectra of **1a** and **1b** obtained under slow MAS conditions (Figure 2b and 3b) give—within the margin of error—a good agreement of the nitrogen–hydrogen distances with those obtained for the static powders. We note, however, that the precision of the data depends on constant spinning speeds, which is a problem especially at low temperatures. The extraction of values of nitrogen–deuterium distances r^{15}_{ND} from sideband spectra, where numerous information is contained in the intensities of a few sidebands, becomes more difficult if there is some doubt about the degree of deuteration. This problem is found to be less severe in the case of a complete line-shape analysis of the spectrum of a static powder.

In particular, we found average dipolar coupling constants corresponding to distances of $r^{15}_{NH} = 1.093 \pm 0.003$ Å for **1a** and $r^{15}_{ND} = 1.079 \pm 0.0015$ Å for **1b**. These values were obtained from six spectra of static and spinning **1a** and seven spectra of static and spinning **1b**, acquired for varying experimental conditions, magnetic fields of 2.1 and 7 T, and different samples. The errors indicate the standard deviations $\sigma = 0.68 \cdot (\sum_{i=1}^{n}(r^i - r)^2/(n-1))^{1/2}$. The obtained value of r^{15}_{NH} as well as the isotropic chemical shift of 4.2 ppm of **1a** and **1b** is somewhat larger than that of $r^{15}_{NH} = 1.075 \pm 0.003$ Å and 2.9 ppm obtained in ref 13a for $(CH_3)_3{}^{15}NH^+{\cdots}Cl$. The difference is real and interesting. We assign it to the existence of different phases[27] of **1**, which, moreover, can contain varying amounts of crystal water.

It is unlikely that the observed difference between r^{15}_{NH} and r^{15}_{ND} in **1a** and **1b** arises from the neglect of dipolar $^{15}N-D$ couplings in **1a** of second-order effects on the dipolar $^{15}N-D$ coupling in **1b**.[20] Firstly, an analysis taking into account the second-order effects on the basis of first-order perturbation treatment[20] shows that the order of magnitude of this effect is small, i.e. about 20 Hz for **1b** at 2.1 T and about 6 Hz at 7 T. Secondly, the second-order induced frequency shifts are zero for the line positions which are important for the distance measurement, i.e. the shoulders in Figure 3a, where the $^{15}N-D$ bond directions are either perpendicular or parallel to the magnetic field. Thirdly, it is well-known[28] that at room temperature the methyl deuterons of **1a** perform rapid jumps around the C–N axis and the methyl groups around the N–H axis. The residual averaged dipolar coupling constant D between the ^{15}N nucleus and a methyl deuteron of **1a** is then only about 35 Hz. This coupling appears in the spectrum of Figure 2a only as a contribution to the line width. In the case of the sideband spectra of **1a** such small couplings can also not be observed, because the contributions to the sideband intensities arising from the spin states with a total magnetic quantum number of $+M$ are compensated by those arising from $-M$. We therefore assign the small difference in r^{15}_{NH} in **1a** and r^{15}_{ND} in **1b** of about 0.015 Å to an H/D isotope effect. This effect is expected for an anharmonic potential for the proton motion leading to a smaller value of r^{15}_{ND} as compared to r^{15}_{NH} resulting from the smaller zero-point energy of the deuteron. Much larger H/D isotope effects on the distances are estimated in stronger hydrogen bonds, which are currently being studied in our laboratory and which will be of interest from a theoretical standpoint.

N–D···N Hydrogen-Bonded Systems Subject to Proton Transfer. Example: Dimethyldibenzotetraaza[14]annulene (2) at 120 and 355 K. Hydrogen-bonded systems of the type N–L···N, L = H, D, are characterized by two nitrogen–deuterium distances, r_{NL} and $r_{L\cdots N}$ and the nitrogen–nitrogen distance r_{NN}. If the hydrogen bond is linear, $r_{NL} + r_{L\cdots N} = r_{NN}$, otherwise $r_{NL} + r_{L\cdots N} > r_{NN}$. If r_{NN} is small, the proton moves in a single-well potential, leading to comparable values of r_{NL} and r_{NN}; if the potential is asymmetric, these distances may be slightly dependent on temperature, and if r_{NN} is large, the system may be subject to a thermally activated proton tautomerism which also modulates the dipolar $^{15}N-L$ coupling. These circumstances all complicate the determination of the above mentioned distances. Therefore, it is important to be able to determine the latter at low temperature, where the protons are localized.

In this section, we show that through the application of low-temperature ^{15}N NMR of static powders it is possible to determine not only the intrinsic distances r_{ND} but also $r_{D\cdots N}$. The system considered here is the ^{15}N-labeled dye dimethyldibenzotetraaza[14]annulene (**2**), whose structure is shown in Figure 4. The molecule contains two equivalent N–L···N units, in which a fast double proton transfer takes place at room temperature.[9a,10b] By ^{15}N CPMAS NMR both N–L···N units are found to be equivalent and only two tautomeric states were observed, to which the structures shown in Figure 3 were assigned. Recently, the X-ray crystal structure of **2** was determined.[29] The molecule is planar, and the distance r_{NN} across the two hydrogen bonds is 2.75 Å. In the following, we denote the nitrogen atoms of the N–L···N units in state 1 bound

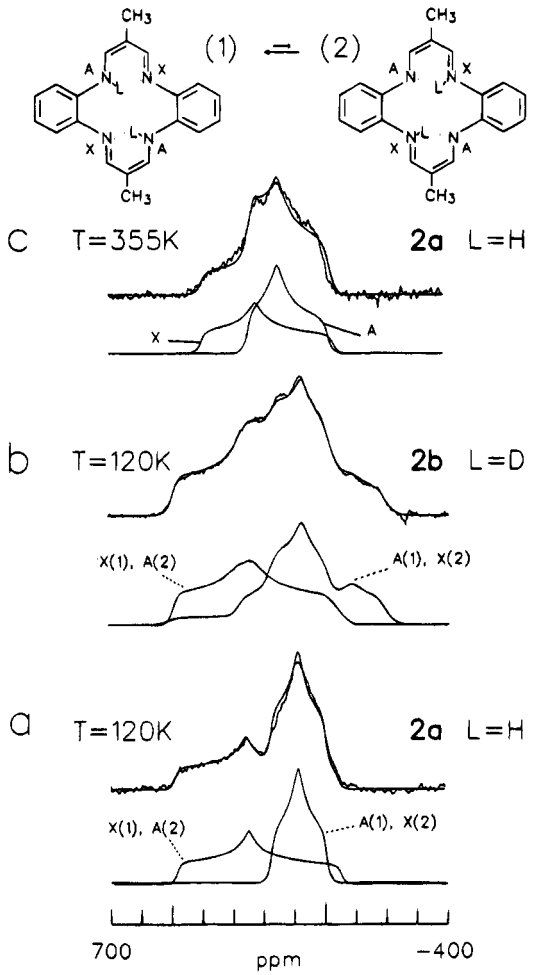

Figure 4. Experimental and calculated 9.12 MHz ^{15}N CP NMR spectra of a static powder of ^{15}N-enriched **2**. The calculated subspectra for the various nitrogen atoms are included. (a) **2a** (L = H) at 120 K, 14 mg of substance, number of scans 8000, 3 s repetition time, 6 ms CP time. The exchange between the tautomeric states 1 and 2 is slow within the NMR time scale. (b) **2b** (L = D) at 120 K; 40 mg of substance was deuterated in a mixture of CH_2Cl_2/CH_3OD and filled in the rotor under nitrogen to prevent reprotonation; CP time 13 ms, 3 s repetition time, number of scans 7000. The other parameters used for the calculation of all spectra are the same as given in Table 1. (c) **2a** at 355 K; the exchange between 1 and 2 is fast within the NMR time scale. Equilibrium constant of tautomerism $K_{12} = 0.353$,[13] $\alpha^S_{cs}(1) = 0°$, $\beta^S_{cs}(1) = 0°$, and $\gamma^S_{cs}(1) = 0°$; $\alpha^S_{cs}(2) = -37°$, $\beta^S_{cs}(2) = 0°$, and $\gamma^S_{cs}(2) = 0°$.

to the light isotope L as A and the other nitrogens as X. The tautomerism between states 1 and 2 can thus be written as (1) A—L⋯X ⇌ (2) A⋯L—X, S = A, X = ^{15}N. Due to molecular interactions, the gas-phase degeneracy of the two structures is lifted in the solid state. Below 120 K the mole fraction $x(1)$ of tautomer 1 is $x(1) > 0.96$.[10b] Moreover, the forward and the backward reaction rate constants are slow in comparison to the NMR time scale. The CPMAS spectra then exhibit two sharp singlets for the protonated and the nonprotonated nitrogen atoms.[10b] In contrast, at room temperature both tautomers exchange fast on the NMR time scale. In the CPMAS spectra, the averaged line positions for spin A and spin X are still dissimilar because of the equilibrium constant $K_{12} = x(2)/x(1) \neq 1$.

In a first stage we measured the proton-decoupled CP NMR spectrum of the static powder of the protonated compound **2a**. As shown in Figure 4a, the resulting superposed experimental and calculated spectra consist of two subspectra which exhibit the usual features of a non axially symmetric CSA tensor. The

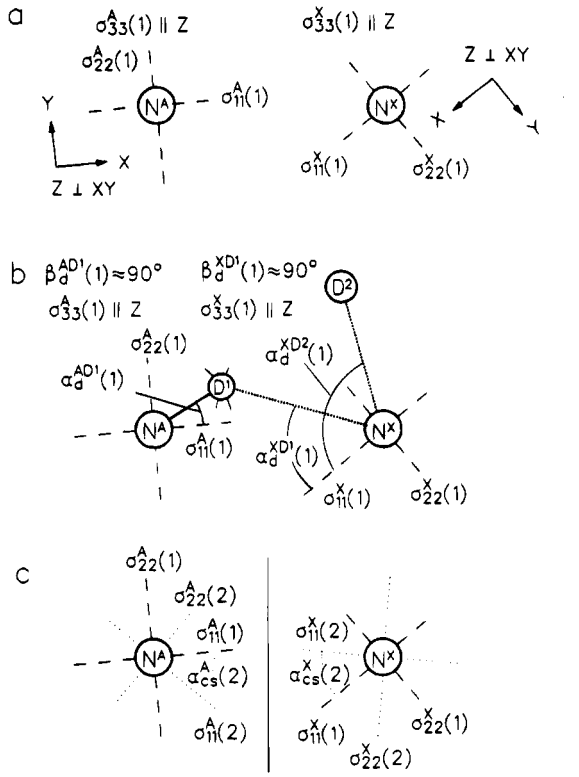

Figure 5. (a) Components of the ^{15}N CSA tensors of **2** arising from the line-shape analysis of Figure 4a. In this stage of analysis the relative positions of the CSA tensors of A and X are not obtained. (b) The position of D^1 determined by the intersection of two cycles with the radii $r_{AD}(1)$ and $r_{XD}(1)$ determined by line-shape analysis of Figure 4b. The angles $\alpha_s^{AD^1}1)$ and $\alpha_d^{XD^1}(1)$ also determined in Figure 4b allow the location of the principal components of the CSA tensors. The elements $\sigma^S_{33}(1)$, S = A, X, are perpendicular to the paper plane. Location of D^2 in the adjacent hydrogen bond; determined by the line-shape analysis. (c) The relative orientation of the CSA tensors of nitrogen atoms A and X resulting from the mirror symmetry between state 1 and state 2.

subspectrum of the nonprotonated nitrogen atoms X appears at lower field and is larger than compared to the spectrum of the protonated nitrogen atoms A. The principal components of the CSA tensors of A and X, which were extracted from the spectrum by line-shape analysis, are depicted in Figure 5a and assembled in Table 1. The relative orientation of both tensors cannot be obtained from Figure 4a. Thus, the tensors of A and X are defined in different unrelated coordinate systems, i.e.

$$\alpha^A_{cs}(1) = 0°, \beta^A_{cs}(1) = 0°, \gamma^A_{cs}(1) = 0°$$

$$\alpha^X_{cs}(1) = 0°, \beta^X_{cs}(1) = 0°, \gamma^X_{cs}(1) = 0° \qquad (10)$$

The coordinate systems were arranged in Figure 5a arbitrarily in such a way that the two Z directions lay parallel.

In the next stage we measured the ^{15}N CP NMR spectrum of the deuterated molecule **2b** at 120 K, shown together with the calculated spectrum and the subspectra in Figure 4b. Since the dipolar interaction of the nitrogen atom X(1) with the two deuterons D^1 and D^2 is small, where D^2 represents the deuteron in the adjacent hydrogen bond, the subspectrum of X is subject only to minor, but nevertheless significant, changes as compared to the corresponding subspectrum of Figure 4a. By contrast, the subspectrum of A(1) is strongly affected by deuteration. The line-shape calculations of Figure 4b were greatly simplified by the knowledge of the parameters of the CSA tensors. Only the nitrogen—deuterium distances $r_{AD^1}(1)$, $r_{XD^1}(1)$, and $r_{XD^2}(1)$ and

TABLE 1: Parameters of Chemical Shielding[a] and Dipolar Coupling in Dimethyldibenzotetraaza[14]annulene (2) Obtained by the Line-Shape Analyses Depicted in Figure 4

$\sigma_{11}^{A}(1) = 169 \pm 2$ ppm $= \sigma_{11}^{X}(2)^b$	$\alpha_{cs}^{A}(1) = \alpha_{cs}^{X}(1) = 0°$
$\sigma_{22}^{A}(1) = 80 \pm 3$ ppm $= \sigma_{22}^{X}(2)^b$	$\beta_{cs}^{A}(1) = \beta_{cs}^{X}(1) = 0°$
$\sigma_{33}^{A}(1) = -11 \pm 2$ ppm $= \sigma_{33}^{X}(2)^b$	$\gamma_{cs}^{A}(1) = \gamma_{cs}^{X}(1) = 0°$
$\sigma_{iso}^{A}(1) = 79$ (78) ppm $= \sigma_{iso}^{X}(2)^b$	$\alpha_{cs}^{A}(2) = \alpha_{cs}^{X}(2) = -37°$
$\sigma_{11}^{X}(1) = 487 \pm 2$ ppm $= \sigma_{11}^{A}(2)^b$	$\beta_{cs}^{A}(2) = \beta_{cs}^{X}(2) = 0°$
$\sigma_{22}^{X}(1) = 256 \pm 2$ ppm $= \sigma_{22}^{A}(2)^b$	$\gamma_{cs}^{A}(2) = \gamma_{cs}^{X}(2) = 0°$
$\sigma_{33}^{X}(1) = -47 \pm 3$ ppm $= \sigma_{33}^{A}(2)^b$	
$\sigma_{iso}^{X}(1) = 232$ (232) ppm $= \sigma_{iso}^{A}(2)^b$	
$\alpha_d^{AD^1}(1) = 28 \pm 2° = \alpha_d^{XD^1}(2)^b$	$\alpha_d^{AD^2}(1) = 23 \pm 9° = \alpha_d^{XD^2}(2)^b$
$\beta_d^{AD^1}(1) = 90 \pm 3° = \beta_d^{XD^1}(2)^b$	$\beta_d^{AD^2}(1) = 90 \pm 15° = \beta XD^2(2)^b$
$\alpha_d^{XD^1}(1) = 57 \pm 4° = \alpha_d^{AD^1}(2)^b$	$\beta_d^{XD^1}(1) = 95 \pm 6° = \beta_d^{AD^1}(2)^b$
$\alpha_d^{XD^2}(1) = 115 \pm 6° = \alpha_d^{AD^2}(2)^b$	$\beta_d^{XD^2}(1) = 98 \pm 7° = \beta_d^{AD^2}(2)^b$
$r_{AD^1}(1) = 1.042 \pm 0.003$ Å $= r_{XD^1}(2)^b$	
$r_{AD^2}(1) = 2.67 \pm 0.16$ Å $= r_{XD^2}(2)^b$	
$r_{XD^1}(1) = 1.92 \pm 0.06$ Å $= r_{AD^1}(2)^b$	
$r_{XD^2}(1) = 2.35 \pm 0.09$ Å $= r_{AD^2}(2)^b$	

[a] Reference: solid $^{15}NH_4Cl$. [b] Values of state 2 resulting from the symmetry between state 1 and state 2. Values in parentheses were obtained by CPMAS. For explanation of symbols see text and Figures 1 and 5.

the polar angles $\alpha_d^{AD^1}(1)$, $\alpha_d^{XD^1}(1)$, $\alpha_d^{XD^2}(1)$, $\beta_d^{AD^1}(1)$, and $\beta_d^{XD^1}(1)$ were varied and determined by line-shape analysis. The parameter values are listed in Table 1. We obtained $\beta_d^{AD^1}(1) \approx \beta_d^{XD^1}(1) \approx 90°$. This result is compatible only with the mirror symmetry in the molecular plane if $\sigma_{33}^{A}(1)$ and $\sigma_{33}^{X}(1)$ are parallel and located perpendicularly to the molecular plane, as depicted in Figure 5b. Using the value of $r_{AX} = 2.75$ Å[29] obtained by crystal structure analysis of **2a**, we were then able to locate D^1 in the hydrogen bond as shown in Figure 5b at the intersection of two cycles, centered in A and X, with the radii of the nitrogen−deuterium distances. Knowledge of the angles $\alpha_d^{AD^1}(1)$, $\alpha_d^{XD^1}(1)$, and $\alpha_d^{XD^2}(1)$ then allowed one to orientate the remaining components of the CSA tensors of A and X in state 1 in the molecular frame as well as D^2 as indicated in Figure 5b. In this figure, the direction of $\sigma_{11}^{A}(1)$ is obtained via the clockwise rotation of the tensor around Z, starting from $\sigma_{11}^{A}(1) \parallel r_{AD^1}(1)$. This choice is arbitrary, and a counterclockwise rotation would also have been possible. A similar ambiguity arises in the orientation of the tensor components of X and the direction of $r_{XD^2}(1)$. Nevertheless, this ambiguity does not influence the localization of D^1 in the hydrogen bond.

In the case of **2**, this ambiguity can be solved because of its tautomerism, as explained in the following. We assume that the tautomers 1 and 2 are related by the reflexion in a mirror plane perpendicular to the molecular plane, as seen from the structural formula in Figure 4. The consequence for the chemical shifts is, for example, the following relations for the isotropic chemical shifts

$$\sigma_{iso}^{A}(1) = \sigma_{iso}^{X}(2) \text{ and } \sigma_{iso}^{X}(1) = \sigma_{iso}^{A}(2) \quad (11)$$

which has previously been shown to hold.[13] It is therefore plausible to assume that these relations are also in keeping with the individual tensor components

$$\sigma_{ii}^{A}(1) = \sigma_{ii}^{X}(2),\ ii = 11, 22, 33 \quad (12)$$

as indicated in Table 1. When the tautomerism occurs, the CSA tensors of nitrogen A and X change their size and orientation. Because of the mirror symmetry in the molecular plane and between the two tautomers 1 and 2, the components $\sigma_{33}^{A}(2)$, $\sigma_{33}^{X}(2)$ must remain parallel to Z, i.e.

$$\beta_{cs}^{A}(2) = 0°, \gamma_{cs}^{A}(2) = 0°, \beta_{cs}^{X}(2) = 0°, \gamma_{cs}^{X}(2) = 0° \quad (13)$$

The tensors of nitrogen A and X in the tautomeric states 1 and 2 are then related by a rotation around Z, described by the angle $\alpha_{cs}^{A}(2) = \alpha_{cs}^{X}(2)$, as illustrated in Figure 5c. Figure 5c depicts graphically that $\alpha_{cs}^{A}(2) \approx -45°$. Returning to the previously mentioned ambiguity, $\alpha_{cs}^{A}(2) \approx 10°$, 67°, and −104° was obtained for the other three arrangements mentioned before.

Now, an experimental value of $\alpha_{cs}^{A}(2)$ could be obtained by line-shape analysis of the ^{15}N CP spectrum of **2a** at 355 K, as shown in Figure 4c. At this temperature, the tautomerism between tautomers 1 and 2 lies in the nanosecond time scale.[10b] Due to the different energies of both tautomers in the solid state, the spectrum consists of two different subspectra for nitrogen atoms A and X, where A is characterized by a higher average proton density. With the knowledge of the equilibrium constant[10b] at 355 K, $K_{12} = 0.363$, the spectrum of Figure 4c could be simulated by using fixed values for all tensor parameters obtained from Figure 4a,b, only by setting $\alpha_{cs}^{A}(2) = -37 \pm 6°$. This value is only compatible with the value of −45° graphically obtained for the arrangement shown in Figure 5b, thus resolving the above mentioned ambiguity on the orientations of the CSA tensors in the molecular frame.

From the analysis of the ^{15}N T_1 data of solid **2**,[10b] using the value for the NN distance $r_{AX} = r_{NN} = 2.75$ Å, we obtained a nitrogen−hydrogen distance of $r_{AH^1}(1) = r_{XH^1}(2) = 1.036 \pm 0.006$ Å. Within the margin of error, this value coincides with the value of $r_{AD^1}(1) = 1.042 \pm 0.003$ Å obtained here. However, the results of both methods should not be interpreted in terms of an H/D isotope effect on the N−L bond distances because of the entirely different methods employed, which could be affected by different systematic errors.

The Effect of Hindered Ammonium Group Rotation on the Dipolar ^{15}N−D Coupling. Example: α-Glycine (3). The last example concerns the geometry and the mobility of the ammonium group in α-glycine, $^-OOCCH_2{}^{15}NL_3^+$ (**3**), L = H, D, abbreviated in the following also as RNL_3. Depending on the degree of deuteration, the ^{15}N nucleus studied is dipolar coupled either to zero, one, two or three deuterons D^i, $i = 1, 2, 3$. Thus, the species RNH_3 (**3a**), RNH_2D (**3b**), $RNHD_2$ (**3c**), and RND_3 (**3d**) have to be taken into account. In the case of a statistical distribution, the mole fractions of the various isotopic species are given by $x_{RNH_3} = (1 - D)^3$, $x_{RNH_2D} = 3(1 - D)^2D$, $x_{RNHD_2} = 3(1 - D)D^2$, and $x_{RND_3} = D^3$, where D represents the deuterium fraction in the ammonium site. In other words, the populations of the various species can be described in terms of a single parameter, D.

A computer program was written which enabled us to calculate the ^{15}N line shapes for **3a**−**3d** in the absence and presence of 3-fold rotational jumps around the C−N axis. Several results are depicted in Figure 6. In order to demonstrate the principal line-shape features, the residual line width chosen was relatively small. In the case of a vanishing chemical shift anisotropy, the species RNH_3 contributes only a single line to the spectra because of ^1H decoupling. The species RNH_2D contributes a Pake triplet, shown in Figure 6a. For the calculation of the spectra of the species $RNHD_2$ and RND_3 the various D^i−N−D^j bond angles must be specified. In the calculations we assumed a C_3 symmetry of the ammonium group; that is, we set the angles relating the dipolar tensors of the different deuterons as $\alpha_d^{ND^1} = 0°$, $\alpha_d^{ND^2} = 120°$, and $\alpha_d^{ND^3} = 240°$ and $\beta_d^{ND^1} = \beta_d^{ND^2} = \beta_d^{ND^3} = \beta_d^{ND} = 70.5°$, corresponding to a tetrahedral symmetry of the ammonium group.

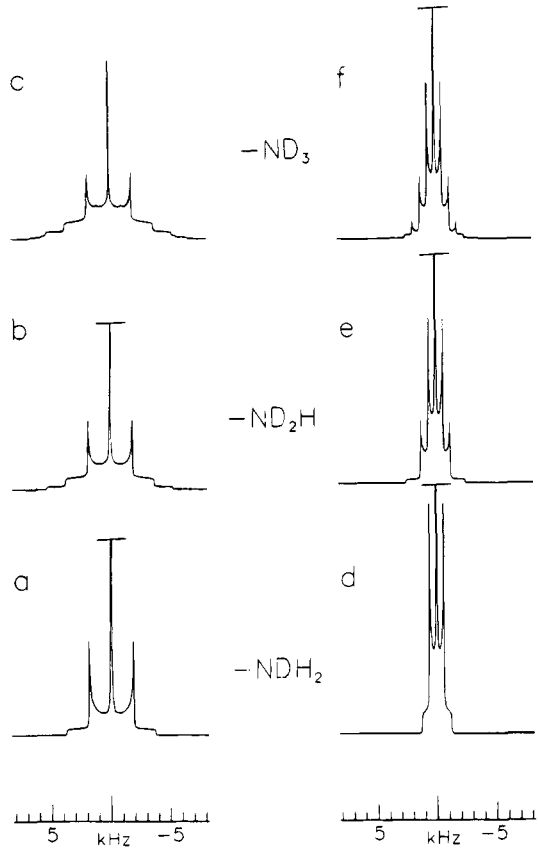

Figure 6. Calculated ^{15}N Static powder spectra of the ammonium group for different isotopic species $RND_{3-n}H_n$. Tetrahedral geometry and absence of a chemical shift anisotropy are assumed; $r_{ND} = 1$ Å. Left column depicts the rigid case; right column is calculated for the case of a fast rotation about the 3-fold axis.

Furthermore, all ND distances were set to 1 Å. The resulting spectrum for $RNHD_2$ is shown in Figure 6b and the spectrum of RND_3 in Figure 6c. As the number of deuterons is increased, the number of singularities increases; however, they are barley perceptible and the central "triplet" parts of the patterns are not particularly altered. However, the number of shoulders on the high- and low-frequency sides of the center band is different. Since the total intensity is identical for all patterns, line intensity is shifted from the line center to the outer wings as the number of deuterons is increased, thus reducing the intensity ratio between the center band and the outer maxima.

In view of previous observations by ^2H NMR showing that the ammonium group of **3** is subject to 3-fold rotational jumps characterized by correlation times of picoseconds at room temperature,[17] we calculated the powder ^{15}N NMR spectra of **3b**−**3d** for this particular case; the results are depicted in Figure 6d,e. The spectra are pure Pake multiplets and resemble those in Figure 6a−c, but the signal widths are reduced by a factor of 0.34. When larger residual line widths are introduced, only single broad lines result, where the overall line width increases with the number of attached deuterons because of the larger multiplet widths.

Figure 7a,c shows the superposed experimental and calculated ^{15}N CP NMR spectra of a static powder of **3** at 112 K with deuterium fractions of $D \approx 0.22$ and $D \approx 0.8$. As in Figure 6, a C_3 symmetry of the ammonium group was assumed for $RNHD_2$ and RND_3, i.e. $\alpha_d^{ND^1} = 0°$, $\alpha_d^{ND^2} = 120°$, and $\alpha_d^{ND^3} = 240°$, but $\beta_d^{ND^1} = \beta_d^{ND^2} = \beta_d^{ND^3} = \beta_d^{ND}$ was a parameter of the simulation, as well as the ND distance. At $D \approx 0.22$ and 112 K (Figure 7a) the line shape dominantly consists of a center band arising from RNH_3 and a Pake triplet arising from RNH_2D;

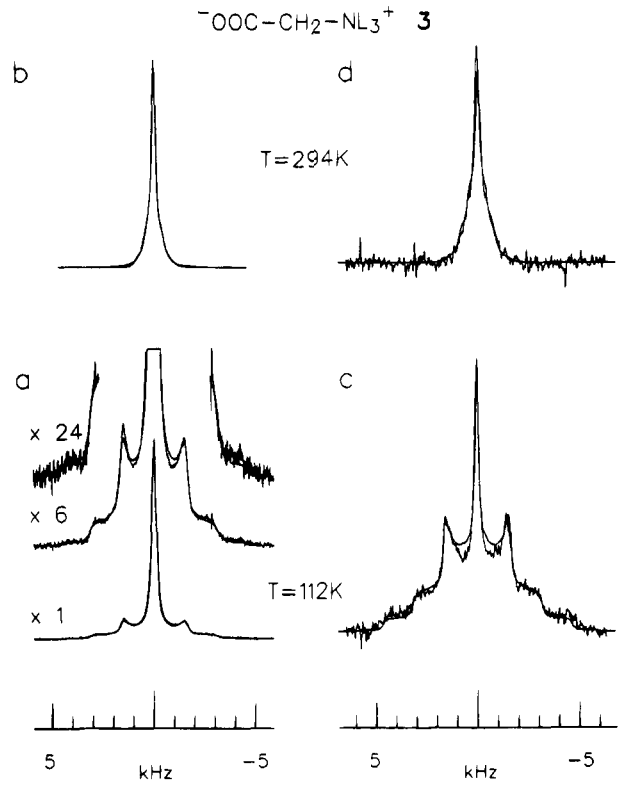

Figure 7. Experimental and calculated ^{15}N powder spectra of partially deuterated ^{15}N-labeled glycine at 9.12 MHz and different deuterium fractions. (a,b) $D \approx 0.22$, mole fractions of $x_{RNH_3} = 0.5$, $x_{RNH_2D} = 0.34$, and $x_{RNHD_2} = 0.15$, 5 ms CP time, 3 s repetition time, number of scans 8000; (a) spectrum at 112 K, (b) spectrum at room temperature. $\sigma_{11} = -8$ ppm, $\sigma_{22} = -8$ ppm, $\sigma_{33} = 4$ ppm, $\sigma_{iso}^{mas} = -6$ ppm, $\alpha_d^{ND^1} = 0°$, $\alpha_d^{ND^2} = 120°$, $\alpha_d^{ND^3} = 240°$ $\beta_d^{ND^i} = 68°$, and $r_{ND^i} = 1.058$ Å (c,d) $D > 0.8$, mole fractions of $x_{RNHD_2} = 0.45$, $x_{RND_3} = 0.55$; the experimental mole fractions are likely distorted by cross polarization effects; CP time 10 ms, 5 s repetition time, number of scans 10 000; (c) spectrum at 112 K, (d) spectrum at room temperature. $\sigma_{11} = -6$ ppm, $\sigma_{22} = -6$ ppm, $\sigma_{33} = -6$ ppm, $\sigma_{iso}^{mas} = -6$ ppm, $\alpha_d^{ND1} = 0°$, $\alpha_d^{ND^2} = 120°$, $\alpha_d^{ND^3} = 240°$, $\beta_d^{ND^i} = 68°$ in c and 69° in d, and $r_{ND^i} = 1.049$ Å.

it is almost independent of the above mentioned angles. The small population of $RNHD_2$ leads to the outer shoulders depicted in the vertically expanded spectrum of Figure 7a. At $D \approx 0.8$ and 112 K (Figure 7c), approximately 50% of the signal consists of a pattern arising from RND_3 and around 40% from a pattern arising from $RNHD_2$ (**3c**), as shown in Figure 6. Two high- and low-field shoulders are observed, whereas further details of the pattern in Figure 6c are lost in the noise. However, the intensity ratio between the shoulders, the center band, and the outer maxima is characteristic, and the altogether larger signal width as compared to Figure 7a is well reproduced. From the simulations of the spectra at 112 K we find—within the margin of error—equal distances between ^{15}N and all three deuterons. In particular, we obtain $r_{ND^i} = 1.058 \pm 0.003$ Å from the spectrum in Figure 7a and $r_{ND^i} = 1.049 \pm 0.005$ Å from Figure 7c. The azimuthal angle $\beta_d^{ND} = 68 \pm 2°$ shows a slight deviation from an ideal tetrahedral symmetry.

At room temperature the broad patterns collapse into sharper Pake multiplets which appear due to the overall line width as single lines consisting of a sharp and a broad component; the latter is broader and more intense at high deuterium fractions. These observations are well reproduced by the spectra in Figure 6d−f; that is, they confirm the presence of the 3-fold rotational jumps. In the calculations of the spectra shown in Figure 7b,d only the rotational angle β^{rot} was varied and found to be 68 ± 1° in the case of Figure 7b and 69 ± 1° of Figure 7d. In other

words, it was found that β^{rot} is equal to the value of β_d^{ND} extracted from the low-temperature spectrum of Figure 7c. Note that the rotational jumps observed are stochastic; the influence of a possible quantum rotational tunneling process on the spectra which could take place at very low temperatures was not taken into account.

It is interesting to compare the distances obtained to those derived in a previous neutron diffraction study of α-glycine.[16] In that study it was shown that the three protons of the ammonium group are not equivalent, since three different N−H bond lengths, 1.03, 1.04, and 1.06 Å, were observed. In Figure 7a,c, these small bond length variations are not resolved, but these variations could be the reason for the relatively large residual line width, besides the effects of the chemical shift anisotropy. The values of $r_{^{15}ND}$ derived, therefore, represent average values which are somewhat larger than those obtained in the neutron diffraction study, a phenomenon which has already been discussed above.

Finally, we note that in a biological solid an ammonium group could be subject to an isotropic motion and/or to proton/deuteron exchange processes. Both processes would lead to a complete collapse of the powder ^{15}N NMR signal to a single line. In favorable cases, however, both processes could be distinguished by variable temperature line-shape analysis.

Conclusions

We have shown that it is possible to study the dipolar $^{15}N-D$ interaction in static organic powders by ^{15}N CP NMR and to determine $^{15}N-D$ distances up to 2 Å by line-shape analysis. $^{15}N-D$ spin pairs in organic compounds are conveniently prepared by specific labeling of the desired nitrogen position with ^{15}N and by exchange of the mobile protons by deuterons. Complications arising from the interference of the dipolar interaction with the chemical shift anisotropy can be alleviated by studying the corresponding protonated systems under the condition of proton decoupling. Short $^{15}N-D$ distances can be obtained with a precision of better than 0.01 Å. This method complements ^{15}N NMR techniques which allow the determination of $^{15}N-H$ distances whereby, however, the dipolar coupling between the protons must be removed. In the present work, this condition was achieved simply by full deuteration except the proton site of interest. Thus, for the first time, an H/D isotope effect on the distance between a nitrogen and an attached hydrogen-bonded proton was measured by NMR. The line-shape method is particularly adapted for low-temperature work necessary for obtaining the intrinsic distances when dynamic phenomena modulate the dipolar $^{15}N-H$ and $^{15}N-D$ coupling at room temperature. Such experiments will be especially fruitful for comparative studies by NMR and inelastic neutron scattering.[3] H/D isotope effects obtained by dipolar NMR will constitute interesting information useful for a better understanding of hydrogen bonds, especially if they are strong.

Acknowledgments. We thank the Deutsche Forschungsgemeinschaft, Bonn-Badgodesberg, and Fonds der Chemischen Industrie, Frankfurt, for financial support.

References and Notes

(1) Schuster, P., Zundel, G., Sandorfy, C., Eds. *The Hydrogen Bond*; North Holland Publ. Co.: *Amsterdam*, 1976.

(2) (a) Olovsson, I.; Jönsson, P. G. *Ibid.* Chapter 8, pp 393−456. (b) Jones, D. J.; Brach, I.; Roziere, J. *J. Chem. Soc., Dalton Trans.* **1984**, 1795.

(3) Kearly, G. J.; Fillaux, F.; Baron, M. H.; Bennington, S.; Tomkinson, J. *Science* **1994**, *264*, 1285 and references cited therein.

(4) Ubbelohde, A. R.; Gallagher, K. G. *Acta Crystallogr.* **1955**, *8*, 71.

(5) Novak, A. *Structure Bond.* **1974**, *14*, 177.

(6) Limbach, H. H. *Dynamic NMR Spectroscopy in the Presence of Kinetic Hydrogen Deuterium Isotope Effects. NMR Basic Principles and Progress*; Springer: Berlin−Heidelberg−New York, 1990; Vol. 26, Chapter 2.

(7) (a) Limbach, H. H.; Hennig, J.; Kendrick, R. D.; Yannoni, C. S. *J. Am. Chem. Soc.* **1984**, *106*, 4059. (b) Wehrle, B.; Limbach, H. H.; Köcher, M.; Ermer, O.; Vogel, E. *Angew. Chem.* **1987**, *99*, 914; *Angew. Chem., Int. Ed. Engl.* **1987**, *26*, 934. (c) Wehrle, B.; Limbach, H. H. *Chem. Phys.* **1989**, *136*, 223. (d) Schlabach, M.; Wehrle, B.; Braun, J.; Scherer, G.; Limbach, H. H. *Ber. Bunsen-Ges. Phys. Chem.* **1992**, *96*, 822. Braun, J.; Schlabach, M.; Wehrle, B.; Köcher, M.; Vogel, E.; Limbach, H. H. *J. Am. Chem. Soc.* **1994**, *116*, 6593.

(8) (a) Smith, J. A. S.; Wehrle, B.; Aguilar-Parrila, F.; Limbach, H. H.; Foces-Foces, M.; Cano, F. H.; Elguero, J.; Baldy, A.; Pierrot, M.; Khurshid, M. M. T.; Larcombe-McDuall, J. B. *J. Am. Chem. Soc.* **1989**, *111*, 7304. (b) Aguilar-Parrilla, F.; Scherer, G.; Limbach, H. H.; Foces-Foces, M. C.; Cano, F. H.; Smith, J. A. S.; Toiron, C.; Elguero, J. *J. Am. Chem. Soc.* **1992**, *114*, 9657.

(9) (a) Limbach, H. H.; Wehrle, B.; Zimmermann, H.; Kendrick, R. D.; Yannoni, C. S. *Angew. Chem.* **1987**, *99*, 241. *Angew. Chem., Int. Ed. Engl.* **1987**, *26*, 247. (b) Wehrle, B.; Aguilar-Parrilla, F.; Limbach, H. H. *J. Magn. Reson.* **1990**, *87*, 584. (c) Aguilar-Parrilla, F.; Wehrle, B.; Bräunling, H.; Limbach, H. H. *J. Magn. Reson.* **1990**, *87*, 592.

(10) (a) Limbach, H. H.; Wehrle, B.; Schlabach, M.; Kendrick, R.; Yannoni, C. S. *J. Magn. Reson.* **1988**, *77*, 84. (b) Hoelger, C. G.; Wehrle, B.; Benedict, H.; Limbach, H. H. *J. Phys. Chem.* **1994**, *98*, 843.

(11) (a) Kaplan, S.; Pines, A.; Griffin, R. G.; Waugh, J. S. *Chem. Phys. Lett.* **1974**, *25*, 78. (b) Oas, T. G.; Hartzell, C. J.; McMahon, T. J.; Drobny, G. P.; Dahlquist. F. W. *J. Am. Chem. Soc.* **1987**, *109*, 5956. (c) Oas, T. G.; Hartzell, C. J.; Dahlquist, F. W.; Drobny, G. P. *J. Am. Chem. Soc.* **1987**, *109*, 5962. (d) Hartzell, C. J.; Whitefield, M.; Oas, T. G.; Drobny, G. P. *J. Am. Chem. Soc.* **1987**, *109*, 5966. (e) Chu, P. J.; Carvajal, R. R.; Lunsford, J. H. *Chem. Phys. Lett.* **1990**, *175* (4), 407. (f) Curtis, R. D.; Penner, G. H.; Power, W. P.; Wasylishen, R. E., *J. Phys Chem.* **1990**, *94*, 4000. (g) Hiyama, Y.; Niu, C.-H.; Silverton, J. V.; Bavoso, A.; Torchia, D. A. *J. Am. Chem. Soc.* **1988**, *110*, 2378.

(12) Stoll, M. E.; Vega, A. J.; Vaughan, R. W. *J. Chem. Phys.* **1976**, *65*, 4093.

(13) (a) Roberts, J. E.; Harbison, G. S.; Munowitz, M. G.; Herzfeld, J.; Griffin, R. G. *J. Am. Chem. Soc.* **1987**, *109*, 4163. (b) Tekely, P.; Montigny, F.; Canet, F.; Delpuech, J. J. *Chem. Phys. Lett.* **1990**, *175*, 401. (c) Munowitz, M. G.; Griffin, R. G. *J. Chem. Phys.* **1982**, *76*, 2848. (d) Munowitz, M. G.; Aue, W. P.; Griffin, R. G. *J. Chem. Phys.* **1982**, *77*, 1686.

(14) (a) Gullion, T.; Poliks, M. D.; Schaefer, J. *J. Magn. Reson.* **1988**, *80*, 553. (b) Gullion, T.; Poliks, M. D.; Schaefer, J. *J. Magn. Reson.* **1989**, *81*, 196. (c) Gullion, T.; Schaefer, J. In *Advances in Magnetic Resonance*; Warren, W. S., Ed.; Academic Press: San Diego, 1989; Vol. 13. (d) Gullion, T.; McKay, A. R.; Schmidt, A. *J. Magn. Reson.* **1991**, *94*, 362. (e) Schmidt, A.; McKay, R. A.; Schaefer, J. *J. Magn. Reson.* **1992**, *96*, 644.

(15) Copie, V.; Kolbert, A. C.; Drewry, D. H.; Bartlett, P. A.; Oas, T. G.; Griffin, R. G. *Biochemistry* **1990**, *29*, 9176.

(16) Jönsson, P.-G.; Kvick, A. *Acta Crystallogr.* **1972**, *B28*, 1827.

(17) Müller-Rowatt, C.; Haeberlen, U.; Rowatt, J.; Colpa, J. P. *Chem. Phys.* **1985**, *96*, 327.

(18) Mehring, M. *High Resolution NMR in Solids. NMR Basic Principles and Progress*, 2nd ed.; Springer: Berlin−Heidelberg−New York, 1978; Vol. 11.

(19) Hexem, J. G.; Frey, M. H.; Opella, S. J. *J. Chem. Phys.* **1982**, *77* (7), 3847.

(20) Olivieri, A. C.; Frydman, L.; Diaz, L. E. *J. Magn. Reson.* **1987**, *75*, 50.

(21) Sethi, N. K.; Aldermann, D. W.; Grant, D. M.; *Mol. Phys.* **1990**, *71*, 217.

(22) Herzfeld, J.; Berger, A. E. *J. Chem. Phys.* **1980**, *73* (12), 6021.

(23) Zilm, K. W.; Grant, D. M. *J. Am. Chem. Soc.* **1981**, *103*, 2913.

(24) (a) *Organikum*; VEB Deutscher Verlag der Wissenschaften; Berlin 1984. (b) Baron, W.; Hüning, S. *Chem. Ber.* **1957**, *90*, 395.

(25) (a) Lorch, E.; Breitmaier, E. *Chem. Zg.* **1975**, *99*, 87. (b) Breitmeier, E. *Pharm. Unserer Zeit* **1983**, *6*, 161.

(26) Du Bois Murphy, D. J. *J. Magn. Reson.* **1986**, *70*, 307.

(27) Stammler, M.; *J. Inorg. Nucl. Chem.* **1967**, *29*, 2203.

(28) (a) Jurga, S.; Harbison, G. S.; Blümich, B.; Spiess, H. W.; Fujara, F.; Olinger, A.; *Ber. Bunsen-Ges. Phys. Chem.* **1986**, *90*, 1153. (b) Gruwel, M. L. H.; Wasylishen, R. E. *Z. Naturforsch.* **1990**, *45a*, 55.

(29) Lipkowski, J.; Waluk, J.; Hoelger, C. G.; Limbach, H. H. Unpublished results.

(30) Aldermann, D. W.; Solum, M. S.; Grant, D. M. *J. Chem. Phys.* **1986**, *84*, 3717.

(31) Bär, E.; Fuchs, J.; Kolrep, T.; Rieger, D.; Aguilar-Parrilla, F.; Limbach, H. H.; Fehlhammer, W. P. *Angew. Chem.* **1991**, *103*, 88; *Angew. Chem., Int. Ed. Engl.* **1991**, *30*, 80.